

Sound attenuation in the diffusive compressible Euler model

M. L. MORRIS

*independent researcher, Albuquerque, New Mexico, USA,
e-mails: mmorris400@comcast.net, mmorris400@outlook.com*

WE REVISIT THE DIFFUSIVE COMPRESSIBLE EULER (dcE) MODEL of viscous and heat conducting compressible fluid flow, proposed recently by M. Svård to supersede the Navier–Stokes–Fourier (NSF) equations. Here, we use acoustic measurements in gases and liquids from the literature to demonstrate that the dcE model fails to describe sound wave attenuation in general fluids with physical accuracy. It is shown, for example, that the dcE model underestimates the sound attenuation coefficients of air and water at room temperature by about 13% and 51%, respectively.

Key words: sound attenuation in fluids, ultrasonic experiments, alternative fluid dynamics models.



Copyright © 2024 The Author.

Published by IPPT PAN. This is an open access article under the Creative Commons Attribution License CC BY 4.0 (<https://creativecommons.org/licenses/by/4.0/>).

1. Background and introduction

THE DIFFUSIVE COMPRESSIBLE EULER (DCE) MODEL presented in SVÄRD [1], like its earlier version in SVÄRD [2], features a diffusive mass flux and is proposed by its author to supersede the Navier–Stokes–Fourier (NSF) equations for compressible, viscous, and heat conducting fluids. Both versions exhibit the property of weak well-posedness for the ideal gas case¹ and clear numerical advantages stemming from this property have been demonstrated. In [2], the original dcE model – or the Eulerian flow model, as it was then called – featured only one transport parameter, a diffusion coefficient, ν , that was later chosen effectively to be the kinematic viscosity in DOLEJŠÍ and SVÄRD [3] in order to make accurate predictions of the shear-dominated phenomena that were studied there. As such, the dcE model was constructed to give approximately the same solution as the NSF equations for fluid dynamics problems in this category – and so, if one limits the study to these cases, the dcE model appears to be validated. However, acoustic and thermal phenomena must additionally be examined for complete physical model validation – and in MORRIS [4–6] it is shown that the dcE model, in its original form, makes inaccurate predictions to simple problems of both types, significantly underestimating sound attenuation and the magnitude of the heat flux in ideal gases.

¹If temperature-independence of the specific heat is additionally assumed.

Eventually, SVÄRD and MUNTHE [7] conducted their own study of acoustic waves, but the conclusions they reached were uncertain, as the intent behind much of their treatment was to argue that existing sound attenuation data cannot be used reliably to validate fluid dynamics models². The investigation into sound waves and shock waves in [7] did, however, result in a tentative modification proposed to the original dcE model in the form of an additional energy flux with a new transport parameter. In SVÄRD and MUNTHE [7, Sec. 4], the authors discussed the possibility of choosing the new coefficient to match sound attenuation data, but its value ultimately remained unchosen.

In SVÄRD [1] attention has been turned to the dcE model's thermal predictions, which has resulted in the author's decision to include the additional energy flux on a non-tentative basis. Furthermore, the new transport parameter has been chosen definitively in [1, Eq. (10)] in a manner such as to match measurements of heat conduction; such a choice was also suggested in MORRIS [6, Appendix B] for this purpose. Predictions of sound attenuation from the new version of the dcE model are made in SVÄRD [1] as well, along with the claim that it very likely leads to improved accuracy, but without any real comparison to the experimental data available. Also in [1–3], and [7], the dcE model has only been investigated for ideal gases under the constant specific heat assumption, and its predictions of behaviors in other types of Newtonian fluids requires study, as this is an important factor in determining whether or not it is a viable replacement for the traditional model and to help delineate its validity range. Here, we use sound attenuation measurements from the literature to demonstrate that the modification indeed improves dcE predictions in ideal gases when compared to the original dcE model, however is still insufficient to describe acoustic attenuation with quantitative accuracy in general fluids. Furthermore, the modification is observed either to have little effect or worsen predictions in all liquids studied here, except for mercury, when compared to the original dcE model.

For Newtonian fluids in the NSF model, there are three transport parameters: the shear viscosity, the thermal conductivity, and the bulk viscosity, also referred to as the volume or second viscosity. It is common in fluid dynamics to use Stokes' hypothesis – that is, to assume the bulk viscosity is equal to zero. This assumption, of course, has no significance when studying incompressible problems and little effect when focussing on phenomena in which shear and/or thermal effects dominate. In acoustic and light scattering studies from last century up to the present, however, Stokes' hypothesis has been shown to underpredict sound attenuation in virtually all but the ideal noble gases.

²These arguments are extensively aimed at both the acoustic experiments themselves and the interpretation of acoustic data with linearized models, and I feel that it is best to present a detailed critique of these arguments in a separate treatment.

One may set the bulk viscosity equal to zero in equation (3.15), derived below for the NSF attenuation coefficient in the continuum regime, to arrive at what is known as the Stokes–Kirchhoff equation, and in many of the older references on sound wave experiments, its predictions are called the “classical” contribution and the measured differences from it, the “excess” absorption. It was recognized early on that the bulk viscosity parameter could be used to fit the experimental data, and by way of molecular justification, theories based on relaxation processes due to internal degrees of freedom have been advanced. By the middle of last century, Stokes’ hypothesis had been conclusively invalidated for general compressible fluids; and since then, it has become well-understood that, in addition to shear viscosity and thermal conductivity, the bulk viscosity is an important third transport parameter in the NSF equations that warrants study and quantification based on experiments designed to probe acoustic phenomena, see BHATIA [8] for a detailed discussion. Unfortunately, this parameter is not as commonly tabulated as shear viscosity and thermal conductivity. Also, since it is a parameter found by fitting acoustic or light scattering data and computing with formulas that involve other measured quantities with their own experimental uncertainties, the bulk viscosity is generally not as accurate. Ideally, there will be more complete compendiums of bulk viscosities measured in many different gases and liquids over large temperature, pressure, and frequency ranges, but in the meantime there are a number of benchmark studies available for our consideration.

2. Description of a sound wave experiment

There are a variety of different experimental techniques available for researchers to examine acoustic phenomena in fluids, some of which include spherical resonators, acoustic spectroscopy, and Rayleigh–Brillouin light scattering, see [9–11], for example – but the type we describe here for conceptual reference is outlined below.

In experiments like ones performed by GREENSPAN [12, 13], PRANGSMA *et al.* [14], and SCHOTTER [15], a vibrating source of frequency f and amplitude A is used to generate longitudinal waves that travel out into an otherwise quiescent fluid at an equilibrium mass density and temperature state,

$$(2.1) \quad (\rho, T) = (\rho_0, T_0),$$

and amplitude and phase measurements are taken at various distances away from the source in order to characterize the way the fluid attenuates and disperses the waves. These measurements may then be compared to predictions made from a fluid dynamics model, such as NSF or dcE, as a test of its validity.

To keep the concepts and analysis as simple as possible, one makes the following assumptions.

1. The amplitude of the sound waves, A , is small enough so that the problem lies in a regime where the Mach number is much less than 1 – i.e. far from the threshold at which shock waves are created – where thermodynamic parameters do not deviate much from their equilibrium values and we observe only linear behavior.
2. The geometry of the experimental set-up is such that the waves can be considered planar.
3. The data is collected far enough away from the vibrating source so that standing waves do not form between the source and receiver, and also so that boundary layer effects near the source do not play a role.
4. When studying gases comprised of polyatomic molecules, the frequency of the sound waves, f , is chosen far enough in excess of relaxation frequencies.
5. For a given sound frequency, gases are studied at pressures high enough for our problem to lie in the continuum regime, where the NSF equations are generally considered to be valid. This requires the mean free path of the gas to be much smaller than the characteristic wavelength of the sound.

Under assumptions 1–3, this problem can be modeled as one-dimensional, and we may use a simplified analysis in which we study only the propagational part of the wave that arises from the linearized equations of fluid dynamics. Assumption 4 is made in order to avoid any peaks in sound absorption that occur near the relaxation frequencies – see BHATIA [8, Ch. 5.1]. Under assumption 5, the roots to the dispersion relation may be approximated and, as discussed in Appendix A, the second part of assumption 3 is realized for distances outside of the thermal layer.

Figure 1 depicts the geometry of the experiment, where we have assumed the spatial variation to occur in the Cartesian x -variable. The source on the left

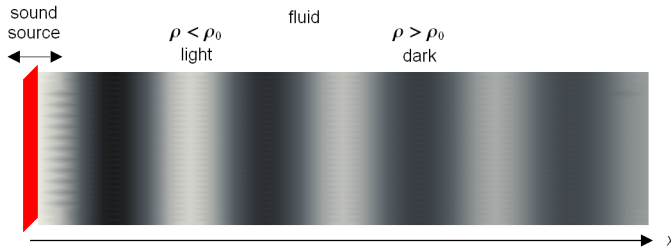


FIG. 1. Planar attenuated sound wave propagating in fluid.

vibrates in the $\pm x$ -direction, causing compression/rarefaction waves to travel through the fluid located on the right. The figure illustrates a snapshot in time, where regions of higher and lower density are indicated as darker and lighter shades, respectively. The wavelength of the sound is the distance between successive dark or light regions – this and the known frequency of the source allow one to compute the sound speed in the fluid. Attenuation in the wave is depicted as the intensity of the shades diminishes farther away from the source.

3. Mathematical models

3.1. Navier–Stokes–Fourier

For the one-dimensional problem considered here, the NSF equations may be expressed as:

$$(3.1) \quad \frac{\partial \rho}{\partial t} = \frac{\partial}{\partial x} \left(-\rho v_x \right),$$

$$(3.2) \quad \frac{\partial(\rho v_x)}{\partial t} = \frac{\partial}{\partial x} \left(-p - \rho v_x^2 + \left(\frac{4}{3}\eta + \zeta \right) \frac{\partial v_x}{\partial x} \right),$$

$$(3.3) \quad \frac{\partial E}{\partial t} = \frac{\partial}{\partial x} \left(- \left(E + p - \left(\frac{4}{3}\eta + \zeta \right) \frac{\partial v_x}{\partial x} \right) v_x + \lambda \frac{\partial T}{\partial x} \right),$$

where, as before, ρ and T represent the mass density and absolute temperature; v_x is the x -component of the fluid velocity; p denotes the thermodynamic pressure; and η , ζ , and λ are used to symbolize the shear viscosity, bulk viscosity, and thermal conductivity, respectively. In addition, E denotes the total energy density:

$$(3.4) \quad E = e + \frac{\rho v_x^2}{2},$$

where the first term on the right-hand side is the internal energy density and the second term, the kinetic energy density.

Sound waves are often studied with the fluid equations cast in a form having the mass density ρ , the temperature T , and the x -component of the fluid velocity v_x , as the dependent variables, and linearized about the constant state,

$$(3.5) \quad (\rho, v_x, T) = (\rho_0, 0, T_0).$$

By expressing the thermodynamic pressure and internal energy density as functions of the mass density and temperature, $p(\rho, T)$ and $e(\rho, T)$, in the Helmholtz free energy representation, one may use techniques as in CALLEN [16] to derive the following differential relationships:

$$(3.6) \quad dp = \frac{c^2}{\gamma} (d\rho + \rho \alpha_p dT)$$

and

$$(3.7) \quad de = \left(\frac{e+p}{\rho} - \frac{T\alpha_p c^2}{\gamma} \right) d\rho + \frac{\rho c_p}{\gamma} dT,$$

where α_p is the thermal expansion coefficient, c is the adiabatic sound speed, c_p is the isobaric specific heat, and $\gamma = c_p/c_v$ is the ratio of isobaric to isochoric specific heats. Substituting (3.4), (3.6), and (3.7) into system (3.1)–(3.3) and linearizing about state (3.5) gives the following system of equations:

$$(3.8) \quad \frac{\partial \rho}{\partial t} = -\rho_0 \frac{\partial v_x}{\partial x},$$

$$(3.9) \quad \frac{\partial v_x}{\partial t} = -\frac{c^2}{\gamma} \left(\alpha_p \frac{\partial T}{\partial x} + \frac{1}{\rho_0} \frac{\partial \rho}{\partial x} \right) + \left(\frac{\zeta + \frac{4}{3}\eta}{\rho_0} \right) \frac{\partial^2 v_x}{\partial x^2},$$

$$(3.10) \quad \frac{\partial T}{\partial t} = \frac{\gamma \lambda}{\rho_0 c_p} \frac{\partial^2 T}{\partial x^2} - \frac{T_0 \alpha_p c^2}{c_p} \frac{\partial v_x}{\partial x},$$

where α_p , c , c_p , γ , η , ζ , and λ are now each understood to be evaluated at the equilibrium thermodynamic state (2.1). If one postulates a plane wave solution to the above that is proportional to

$$(3.11) \quad \exp(kx + i\omega t),$$

where $\omega = 2\pi f$ is the angular frequency of the sound source, then this leads to the following dispersion relation:

$$(3.12) \quad \left(-i \frac{c^2 \lambda}{\rho_0 c_p} + \frac{\gamma \lambda (\zeta + \frac{4}{3}\eta)}{\rho_0^2 c_p} \omega \right) k^4 - \left(c^2 + i \left(\frac{\zeta + \frac{4}{3}\eta + \frac{\gamma}{c_p} \lambda}{\rho_0} \right) \omega \right) \omega k^2 - \omega^3 = 0.$$

In the above, the general thermodynamic relationship,

$$(3.13) \quad \gamma = 1 + \frac{T\alpha_p^2 c^2}{c_p},$$

from CALLEN [16, p. 130] has additionally been used. Equation (3.12) may be solved to obtain four k -roots, and the propagational pair³ is represented as

$$(3.14) \quad k_{pr(\pm)}(\omega) = \pm(\alpha + \beta i)$$

³The other two k -roots pertain to a thermal layer and these are discussed in Appendix A.1.

with the approximate values:

$$(3.15) \quad \alpha = \frac{\omega^2 \eta}{c^3 \rho_0} \left(\frac{2}{3} + \frac{1}{2} \left(\frac{\zeta}{\eta} + \frac{\gamma - 1}{\text{Pr}} \right) \right)$$

and

$$(3.16) \quad \beta = \frac{\omega}{c}.$$

In the above, $\text{Pr} = c_p \eta / \lambda$ represents the Prandtl number, and the approximation is made under the assumption that $\eta \omega / (\rho_0 c^2)$ is small, i.e., that assumption 5 is satisfied and our problem lies in the continuum regime – see Appendix A. Equation (3.15) is the well-known expression for the sound attenuation coefficient, and its frequency squared dependence agrees with experimental observations when assumption 4 is met. The parameters, α and β , can be measured in experiments like those described in Section 2 and, assuming η , γ , and Pr are known independently, a value for ζ can be obtained by matching sound attenuation data. Therefore, the NSF prediction for α given by (3.15) always represents a measured value since it matches the data by design.

Note that the NSF formulas provided above may be used to study any type of Newtonian fluid in the continuum regime – gas or liquid. Note further that we may lift assumption 5 and use the exact propagational roots of dispersion relation (3.12) to study the NSF predictions in gases outside of the continuum regime, however, as demonstrated in Appendix A.3, these predictions become inaccurate for Knudsen numbers roughly greater than 0.1.

3.2. Diffusive compressible Euler

In one spatial dimension, the dcE model proposed in SvÄRD [1] becomes:

$$(3.17) \quad \frac{\partial \rho}{\partial t} = \frac{\partial}{\partial x} \left(-\rho v_x + \nu \frac{\partial \rho}{\partial x} \right),$$

$$(3.18) \quad \frac{\partial(\rho v_x)}{\partial t} = \frac{\partial}{\partial x} \left(-p - \rho v_x^2 + \nu \frac{\partial(\rho v_x)}{\partial x} \right),$$

$$(3.19) \quad \frac{\partial E}{\partial t} = \frac{\partial}{\partial x} \left(-(E + p)v_x + \nu \frac{\partial E}{\partial x} + \kappa_T \frac{\partial T}{\partial x} \right),$$

where ν and κ_T are two transport parameters that the author refers to as the diffusion coefficient and the heat diffusion coefficient. In [1–3], and [7] the system (3.17)–(3.19) is closed with the ideal gas law and under the assumption of temperature-independent specific heat. We do not employ this restriction here and instead test the dcE model for a general fluid as in the previous section. Sub-

stituting (3.4), (3.6), and (3.7) into system (3.17)–(3.19) and linearizing about state (3.5) gives:

$$(3.20) \quad \frac{\partial \rho}{\partial t} = -\rho_0 \frac{\partial v_x}{\partial x} + \nu \frac{\partial^2 \rho}{\partial x^2},$$

$$(3.21) \quad \frac{\partial v_x}{\partial t} = -\frac{c^2}{\gamma} \left(\alpha_p \frac{\partial T}{\partial x} + \frac{1}{\rho_0} \frac{\partial \rho}{\partial x} \right) + \nu \frac{\partial^2 v_x}{\partial x^2},$$

$$(3.22) \quad \frac{\partial T}{\partial t} = -\frac{T_0 \alpha_p c^2}{c_p} \frac{\partial v_x}{\partial x} + \left(\nu + \frac{\gamma \kappa_T}{\rho_0 c_p} \right) \frac{\partial^2 T}{\partial x^2},$$

where α_p , c , c_p , γ , and the dcE diffusion coefficients, ν and κ_T , are understood to pertain to the equilibrium thermodynamic state (2.1). If one postulates a plane wave solution proportional to (3.11) in the above and employs relationship (3.13), then this leads to the dispersion relation,

$$(3.23) \quad i\nu^2 \left(\nu + \frac{\gamma \kappa_T}{\rho_0 c_p} \right) k^6 \left(-ic^2 \left(\nu + \frac{\kappa_T}{\rho_0 c_p} \right) + \nu \left(3\nu + \frac{2\gamma \kappa_T}{\rho_0 c_p} \right) \omega \right) k^4 \\ + \left(-i \left(3\nu + \frac{\gamma \kappa_T}{\rho_0 c_p} \right) \omega - c^2 \right) \omega k^2 - \omega^3 = 0,$$

which yields six k -roots. The propagational pair⁴ is found to be

$$(3.24) \quad k_{pr(\pm)}(\omega) = \pm(\alpha_{\text{dcE}} + \beta_{\text{dcE}}i)$$

with approximate values:

$$(3.25) \quad \alpha_{\text{dcE}} = \frac{\omega^2}{c^3} \left(\nu + \frac{\kappa_T(\gamma - 1)}{2\rho_0 c_p} \right)$$

and

$$(3.26) \quad \beta_{\text{dcE}} = \frac{\omega}{c},$$

under the assumption that $\nu\omega/c^2$ is small, that is, in the continuum regime. From the above, we see that (3.26) gives the same approximation of β as computed from the NSF equations in Section 3.1, and (3.25) is an expression for the sound attenuation coefficient in the dcE model.

Next, note that in order for the dcE model to give accurate predictions of shear phenomena, such as Poiseuille flow and Couette flow in the continuum regime, the diffusion coefficient, ν , must be chosen effectively to equal the kinematic viscosity:

$$(3.27) \quad \nu = \frac{\eta}{\rho}$$

⁴The other two approximate pairs of k -roots are studied in Appendix A.2.

and this is, indeed, how it has been selected in DOLEJŠÍ and SVÄRD [3]. Furthermore, in [1] and [6] it is shown that for the dcE model to make accurate predictions of pure heat conduction, the thermal diffusion coefficient, κ_T , must be chosen effectively as

$$(3.28) \quad \kappa_T = \eta c_p \left(\frac{1}{\text{Pr}} - 1 \right).$$

Thus, one arrives at the following dcE model prediction for the sound attenuation coefficient:

$$(3.29) \quad \alpha_{\text{dcE}} = \frac{\omega^2 \eta}{c^3 \rho_0} \left(1 + \frac{1}{2}(\gamma - 1) \left(\frac{1}{\text{Pr}} - 1 \right) \right),$$

which may be compared directly with measurements of α reported in the literature. Expression (3.29) is the same as the dcE attenuation coefficient presented in SVÄRD [1, Eqs. (11)] after correction⁵ and with parameter \mathbf{c} chosen to equal 1. It is important to note that for substances in which the Prandtl number is greater than 1, such as water, the diffusive heat flux coefficient (3.28) actually becomes negative, a fact that appears to contradict the molecular dynamical theory proposed in SVÄRD [1, Sec. 2]. Therefore, it is of special interest to study acoustic predictions in these cases.

Comparing the above to (3.15), one observes that the ratio of the dcE to measured attenuation coefficients is given by

$$(3.30) \quad \frac{\alpha_{\text{dcE}}}{\alpha} = \frac{\frac{3}{2} - \frac{\gamma}{2} + \frac{(\gamma-1)}{2\text{Pr}}}{\frac{2}{3} + \frac{\zeta}{2\eta} + \frac{(\gamma-1)}{2\text{Pr}}},$$

where, again – since the bulk viscosity, ζ , is chosen to match data from experiments – the NSF value of α is understood to represent the measured value of sound attenuation in the continuum regime. By setting the right-hand side of equation (3.30) equal to 1, one can see that the dcE prediction for sound attenuation is accurate for fluids in which the bulk-to-shear viscosity ratio satisfies the relationship,

$$(3.31) \quad \frac{\zeta}{\eta} = \frac{5}{3} - \gamma.$$

Although the above is satisfied for monatomic ideal gases, where it is appropriate to assume

$$(3.32) \quad \gamma = \frac{5}{3} \text{ and } \zeta = 0,$$

it can easily be demonstrated not to hold for fluids in general.

⁵In both the NSF and dcE formulas in SVÄRD [1, Eqs. (11)], the sound speed squared should be replaced by the sound speed cubed in the denominators.

In the following section, we compare dcE predictions for sound attenuation to measurements in a few different types of fluids. In addition, we compare predictions from the original dcE model [2, 3], referred to below as dcE (old), which can be found by taking $\kappa_T = 0$ instead of Eq. (3.28). From expression (3.25), one computes the attenuation coefficient in this case to be

$$(3.33) \quad \alpha_{\text{dcE(old)}} = \frac{\omega^2 \eta}{c^3 \rho_0},$$

leading to the ratio,

$$(3.34) \quad \frac{\alpha_{\text{dcE(old)}}}{\alpha} = \frac{1}{\frac{2}{3} + \frac{\zeta}{2\eta} + \frac{(\gamma-1)}{2\text{Pr}}}.$$

4. Comparison of model predictions to experimental data

We next compare the theoretical predictions of Section 3 to a sample of sound attenuation measurements in fluids reported in the literature. As explained in Section 1, the errors tend to be quite a bit larger in computed quantities like the bulk viscosity. Therefore, we use direct attenuation measurements, where available, for calculating the model comparison ratios.

4.1. Description of tabulated and plotted data

When studying sound attenuation in a general fluid near an equilibrium thermodynamic state, (ρ_0, T_0) or (p, T_0) , the frequency-independent quantity α/f^2 is often tabulated. Typically in experiments – see HUNTER *et al.* [17, Table II] and HOLMES *et al.* [10, Fig. 2], for example – different frequencies in the range of study are tested to ensure that this quantity indeed has only small variation⁶. From (3.15), (3.29), and (3.33), the theoretical predictions considered here are:

$$(4.1) \quad \frac{\alpha}{f^2} = \begin{cases} (2\pi)^2 \eta \rho_0^{-1} c^{-3} \left(\frac{2}{3} + \frac{1}{2} \left(\frac{\zeta}{\eta} + \frac{(\gamma-1)}{\text{Pr}} \right) \right) & \text{for NSF,} \\ (2\pi)^2 \eta \rho_0^{-1} c^{-3} \left(1 + \frac{1}{2} (\gamma - 1) \left(\frac{1}{\text{Pr}} - 1 \right) \right) & \text{for dcE,} \\ (2\pi)^2 \eta \rho_0^{-1} c^{-3} & \text{for dcE (old),} \end{cases}$$

which we may compare to measured values. In fluids other than ideal noble gases for which it is appropriate to assume $\zeta = 0$, one may set the NSF formula equal to the measured value and, assuming all the other material parameters to be known, solve for the bulk viscosity, ζ , in order to estimate this parameter for the

⁶As mentioned in Section 2, fluids other than ideal noble gases have characteristic relaxation frequencies that must be far enough below the sound source frequency if α/f^2 is to exhibit frequency-independence.

fluid under study; however, in dcE and dcE (old) formulas there are no extra parameters and the predictions are given by their respective formulas in (4.1).

For ideal gases at equilibrium density, ρ_0 , and temperature, T_0 , the pressure and adiabatic sound speed are computed as:

$$(4.2) \quad p = \rho_0 \mathcal{R} T_0$$

and

$$(4.3) \quad c = \sqrt{\gamma \mathcal{R} T_0},$$

respectively, where \mathcal{R} is the specific gas constant. Multiplying (4.1) by the pressure and substituting the above relationships, one finds:

$$(4.4) \quad \frac{\alpha p}{f^2} = \begin{cases} (2\pi)^2 \eta \gamma^{-3/2} (\mathcal{R} T_0)^{-1/2} \left(\frac{2}{3} + \frac{1}{2} \left(\frac{\zeta}{\eta} + \frac{(\gamma-1)}{\text{Pr}} \right) \right) & \text{for NSF,} \\ (2\pi)^2 \eta \gamma^{-3/2} (\mathcal{R} T_0)^{-1/2} \left(1 + \frac{1}{2} (\gamma - 1) \left(\frac{1}{\text{Pr}} - 1 \right) \right) & \text{for dcE,} \\ (2\pi)^2 \eta \gamma^{-3/2} (\mathcal{R} T_0)^{-1/2} & \text{for dcE (old).} \end{cases}$$

In addition to being independent of the frequency when assumption 4 is met, the above quantity is independent of the gas density and not strongly dependent on the temperature since η increases only a bit faster than the square root of temperature most gases. Therefore, in ideal gases, values for $\alpha p / f^2$ are commonly reported.

A typical way of presenting sound attenuation data in gases over large pressure ranges is seen in GREENSPAN [12, Figs. 1–3], [13, Figs. 1–3] and SCHOTTER [15, Figs. 4 and 8]. In each data set used below for Figs. 2–7, the points have been digitized from the original papers in which data was collected at various gas pressures, and measurements corresponding to the dimensionless sound attenuation coefficient,

$$(4.5) \quad \frac{\alpha}{\beta_0} = \frac{c\alpha}{\omega},$$

were plotted versus a dimensionless rarefaction parameter on a log-log scale. In the above, $\beta_0 = \omega / c$ is 2π divided by the sound wavelength when there is no dispersion. The dimensionless rarefaction parameter used in SCHOTTER [15] is $\omega \tau_c$ —where $\tau_c = \eta / p$ is the characteristic time between binary collisions for Maxwell molecules— and the dimensionless (inverse) rarefaction parameter used in GREENSPAN [12, 13] is $r = p / (\omega \eta)$, which upon substitution of (4.2) for ideal gases becomes

$$(4.6) \quad r = \frac{\mathcal{R} \rho_0 T_0}{\omega \eta}.$$

For ideal gases, the parameters, $\omega\tau_c$ and r , are related to each other and the Knudsen number via

$$(4.7) \quad \omega\tau_c = r^{-1} = \sqrt{\frac{2\gamma}{\pi}} \text{Kn},$$

when the Knudsen number is defined as (A.4) in Appendix A. Note that the data points digitized from GREENSPAN [12, 13] were originally plotted versus r , but in Figs. 3–6 below we have replotted them versus r^{-1} to resemble the figures from SCHOTTER [15].

Using the definitions above for α/β_0 and r^{-1} , together with relationships (4.2) and (4.3) and continuum regime approximations (3.15), (3.29), and (3.33) for the model sound attenuation coefficients, one arrives at the following theoretical predictions in ideal gases:

$$(4.8) \quad \frac{\alpha}{\beta_0} = \begin{cases} \gamma^{-1} \left(\frac{2}{3} + \frac{1}{2} \left(\frac{\zeta}{\eta} + \frac{\gamma-1}{\text{Pr}} \right) \right) r^{-1} & \text{for NSF,} \\ \gamma^{-1} \left(1 + \frac{1}{2} (\gamma-1) \left(\frac{1}{\text{Pr}} - 1 \right) \right) r^{-1} & \text{for dcE,} \\ \gamma^{-1} r^{-1} & \text{for dcE (old).} \end{cases}$$

Therefore, the graphs of α/β_0 versus r^{-1} in the continuum regime are lines, as shown in the log-log plots of Figs. 3–6. One may then find the best linear fit to the data, set its slope, m , equal to the NSF slope in (4.8), and solve for the bulk viscosity, assuming that all of the other fluid parameters are known. The foregoing procedure leads to the following equation for the bulk-to-shear viscosity ratio:

$$(4.9) \quad \frac{\zeta}{\eta} = 2\gamma m - \frac{4}{3} - \frac{\gamma-1}{\text{Pr}}.$$

Also, the NSF formulas in (4.4) and (4.8), together with the definitions of parameters β_0 and r above and ideal gas equation (4.2) for the sound speed c , imply the relationship,

$$(4.10) \quad \frac{\alpha p}{f^2} = \frac{(2\pi)^2 m \eta}{\sqrt{\gamma \mathcal{R} T_0}}.$$

To study classical monatomic ideal gases, one takes the ratio of specific heats to be $\gamma = 5/3$ and – if the molecules are assumed to be Maxwellian – the transport coefficient relationships,

$$(4.11) \quad \zeta = 0 \quad \text{and} \quad \text{Pr} = 2/3,$$

leading to the following theoretical predictions from (4.8):

$$(4.12) \quad \frac{\alpha}{\beta_0} = \begin{cases} (7/10)r^{-1} & \text{for NSF and dcE,} \\ (3/5)r^{-1} & \text{for dcE (old).} \end{cases}$$

Notice the above formulas in (4.12) apply to all of the noble gases. Figure 2 contains noble gas measurements from SCHOTTER [15, Figs. 4 and 8]. The dimensionless sound attenuation coefficient, α/β_0 , and the dimensionless inverse sound speed, β/β_0 , are plotted versus the dimensionless rarefaction parameter, r^{-1} , for helium, neon, argon, and krypton at $T_0 = 296$ K on a log-log scale, and as we can see, each of the noble gases indeed falls more or less on the same curves, especially in the low r^{-1} region. The data points extend into the transitional regime, as well, which begins a little after the value $r^{-1} = 0.1$, where we can see α/β_0 begins to deviate from linear and β/β_0 starts to decrease below 1. In Appendix A.3, we lift assumption 5 and use the full propagational roots of dispersion relations (3.12) and (3.23), instead of the approximate roots for small Knudsen numbers, so that we may examine NSF and dcE predictions outside of the continuum regime. There, we observe the failure of both models to describe sound waves in gases when the pressures become too low. This is to be expected since the NSF and dcE models were both formulated as systems of balance laws appropriate only for small Knudsen numbers.

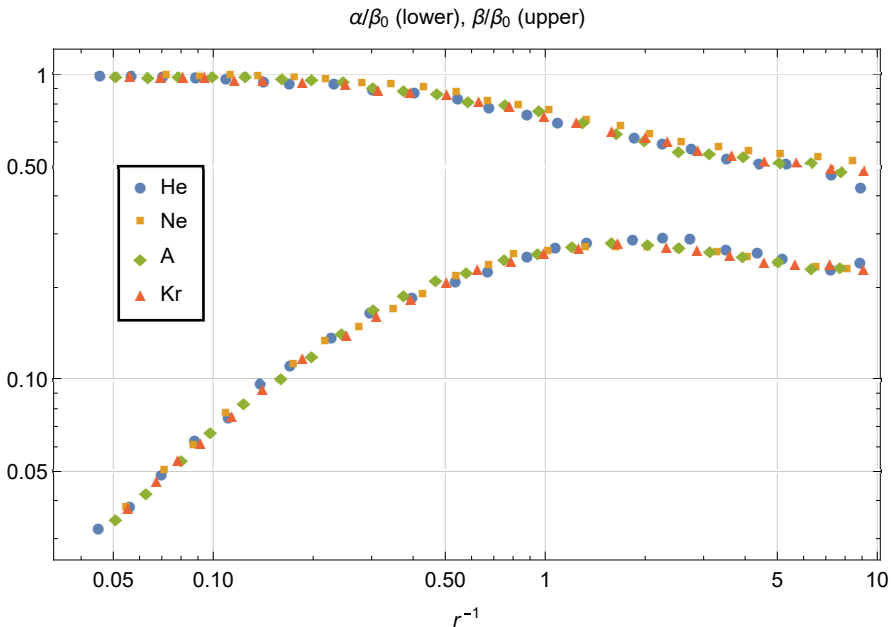


FIG. 2. Dimensionless sound attenuation coefficient and dimensionless inverse sound speed vs. dimensionless rarefaction parameter: noble gas data at 296 K from SCHOTTER [15].

4.2. Monatomic ideal gases

As discussed in Section 3.2, we take (3.32) for ideal noble gases in ratio (3.30), to find

$$\frac{\alpha_{\text{dcE}}}{\alpha} = 1,$$

showing that the current version of the dcE model now gives accurate predictions of sound attenuation in this case. For comparison, taking (3.32) in ratio (3.34) gives

$$\frac{\alpha_{\text{dcE(olD)}}}{\alpha} = \frac{6}{7},$$

which demonstrates the original dcE model underestimates the sound attenuation in ideal noble gases, a fact that has been pointed out previously in MORRIS [4] and [5].

In PRANGSMA *et al.* [14] it is mentioned that surveys of sound attenuation measurements in noble gases after the year 1953 (and before 1973 when the article was published) show agreement to within 3%. Furthermore, these authors report their own experiments in neon at 77.1 K to yield a measured value⁷ of $\alpha p/f^2 = 0.143 \pm 0.001 \text{ atm} \cdot \text{cm}^{-1} \cdot \text{MHz}^{-2}$, which agrees well with their reported theoretical value⁸ of $\alpha p/f^2 = 0.142 \text{ atm} \cdot \text{cm}^{-1} \cdot \text{MHz}^{-2}$. The previous result was used to confirm that their experimental apparatus was functioning properly before using it to take measurements in polyatomic gases, a sample of which is provided in Section 4.3 below.

In Figure 3, we compare the theoretical predictions (4.12) to sound attenuation data measured in the noble gases from GREENSPAN [12] and SCHOTTER [15]. The former ultrasound experiments were performed at the frequency $f = 11 \text{ MHz}$ in helium, neon, argon, krypton, and xenon and at room temperature⁹, and the latter were conducted at $f = 0.975 \text{ MHz}$ in helium, neon, argon, and krypton at temperature $T_0 = 296 \text{ K}$. In Fig. 3, we display only the α/β_0 data points in the lower Knudsen number regime corresponding to $r^{-1} \lesssim 0.125$, which includes the continuum regime and the onset of the transition regime (see Appendix A) – the green points have been digitized from GREENSPAN [12, Fig. 1 (He at $f = 11 \text{ MHz}$), Fig. 2 (Ne and Ar), and Fig. 3 (Kr and Xe)] and replotted versus r^{-1} and the red points, digitized from SCHOTTER [15, Fig. 4 (He) and Fig. 8 (Ne, Ar, and Kr)]. The lines in Fig. 3 correspond to the theoretical

⁷The measurement represents an average of data points at pressure and frequency values corresponding to the continuum regime.

⁸The theoretical value was computed from the NSF formula in (4.4) using tabulated data for all gas parameters except the bulk viscosity, which was assumed equal to zero.

⁹The averages of the temperature ranges reported in [12, Sec. III (B)] are $T_0 = 304, 305, 303, 306, \text{ and } 304 \text{ K}$, for helium, neon, argon, krypton, and xenon, respectively.

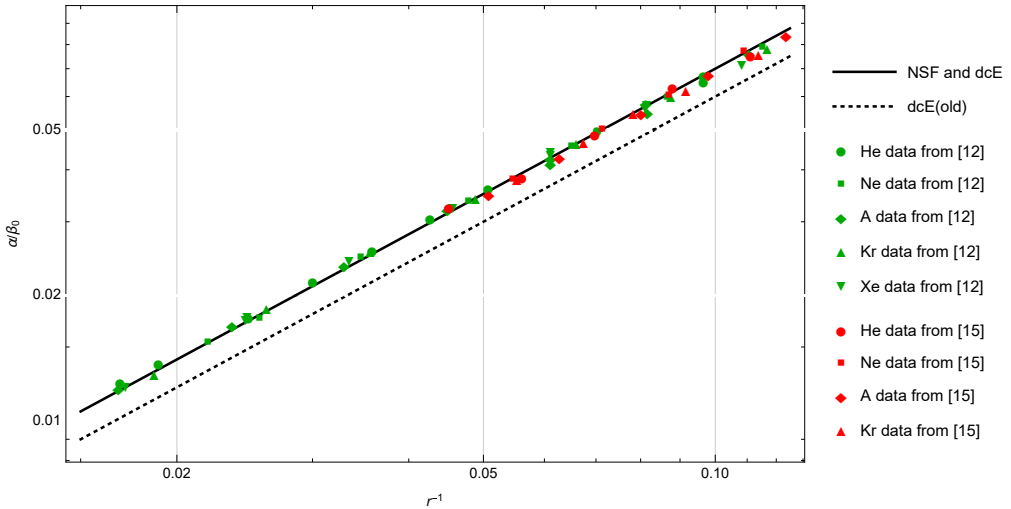


FIG. 3. Dimensionless sound attenuation coefficient vs. dimensionless rarefaction parameter: data and theoretical predictions in the noble gases at room temperature.

predictions of α/β_0 in (4.12), and we can see that the NSF and dcE models provide a good match to the data, whereas the curve predicted by the original dcE model lies well below the measurements¹⁰.

4.3. Polyatomic ideal gases

Please note that here we use the term “polyatomic” to refer to any substance that is not monatomic. In Figs. 4–6, we compare the theoretical predictions from (4.8) to sound attenuation data measured in nitrogen, oxygen, and dry air from GREENSPAN [13], where the ultrasonic experiments were conducted again with frequency $f = 11$ MHz and at room temperature. Figures 4–6 contain only the α/β_0 data in the continuum regime corresponding to $r^{-1} \lesssim 0.05$. The points were digitized from GREENSPAN [13, Figs. 1–3] and replotted versus r^{-1} , and the lines correspond to the formulas for α/β_0 given in (4.8) with the values listed in Table 1 – the temperatures in the second column are averages of the ranges reported for each gas in [13, Sec. III (B)]; the ratios of specific heats in the third column are taken from [18–20]; the Prandtl numbers in the fourth column appear in [13, p. 158]; and the values for the bulk-to-shear viscosity ratio in

¹⁰Although it was not yet standard practice to include error bars during the time of these studies, the quality of the measurements can be deduced from the low scatter exhibited in the data points. Furthermore, the good agreement among data from each of the noble gases and between the two studies in regions where the measurements overlap means large systematic errors are not likely to be present.

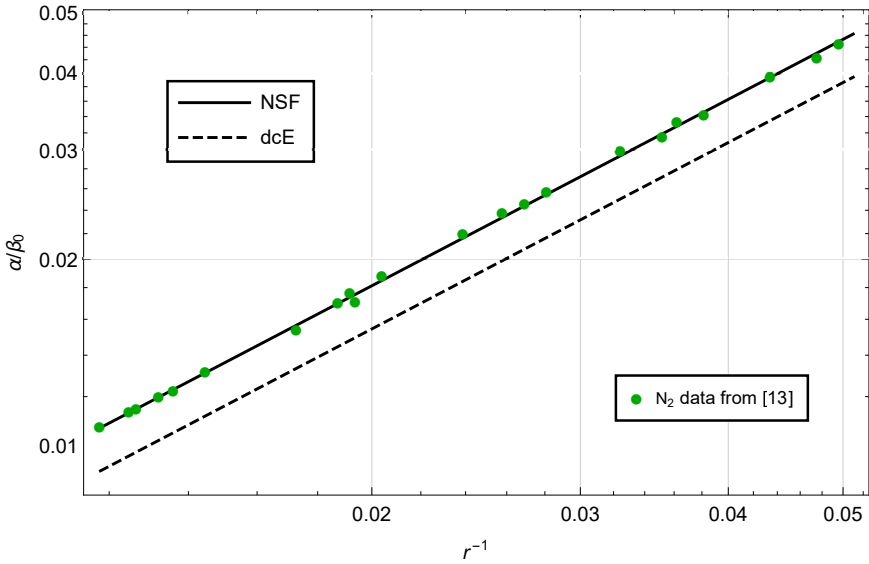


FIG. 4. Dimensionless sound attenuation coefficient vs. dimensionless rarefaction parameter: data and theoretical predictions in nitrogen gas at room temperature.

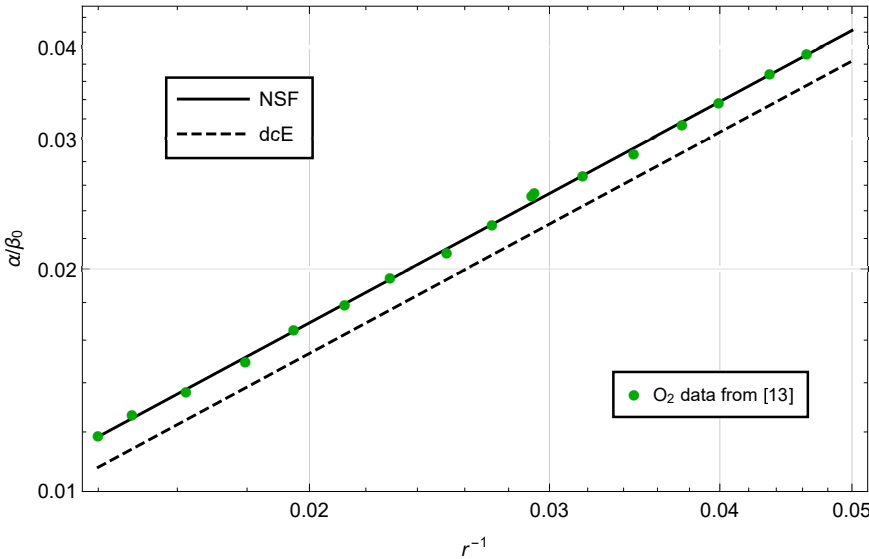


FIG. 5. Dimensionless sound attenuation coefficient vs. dimensionless rarefaction parameter: data and theoretical predictions in oxygen gas at room temperature.

the fifth column are found by fitting lines through the α/β_0 versus r^{-1} data, which yields slopes of $m = 0.906, 0.845,$ and 0.886 for nitrogen, oxygen, and air, respectively, and employing formula (4.9). One observes from Figs. 4–6 and the

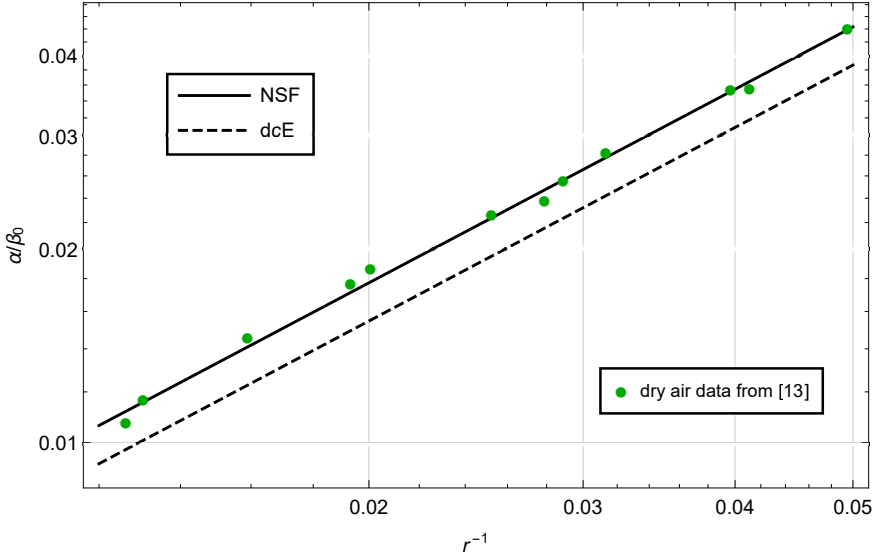


FIG. 6. Dimensionless sound attenuation coefficient vs. dimensionless rarefaction parameter: data and theoretical predictions in dry air at room temperature.

last two columns of Table 1 that in each gas, although the new version is an improvement over the original, there is still significant underestimation of the sound attenuation predicted by the dcE model.

TABLE 1. Nitrogen, oxygen, and air data near room temperature from [13].

Gas	T_0 (K)	γ	Pr	ζ/η	$\alpha_{\text{dcE(oid)}}/\alpha$	$\alpha_{\text{dcE}}/\alpha$
N ₂	304	1.40	0.713	0.643	0.788	0.852
O ₂	302	1.40	0.729	0.483	0.846	0.909
dry air	304	1.40	0.708	0.584	0.806	0.872

Using Eq. (4.10) with the fitted slope to Greenspan’s air data given above, along with the shear viscosity¹¹, $\eta = 1.87 \times 10^{-5} \text{ kg} \cdot \text{m}^{-1} \cdot \text{s}^{-1}$, and specific gas constant of air, $\mathcal{R} = 287 \text{ J} \cdot \text{kg}^{-1} \cdot \text{K}^{-1}$, one computes $\alpha p/f^2 = 1.87 \times 10^{-6} \text{ Pa} \cdot \text{s}^2$. For comparison, calculators [21] and [22] for sound absorption in air can be employed with Greenspan’s experimental parameters¹² to find the value, $\alpha p/f^2 = 1.90 \times 10^{-6} \text{ Pa} \cdot \text{s}^2/\text{m}$, which is about 1.6% higher than Greenspan’s. We estimate

¹¹This value was computed at temperature 304 K using Sutherland’s formula with constants for air given in [13, Sec. III (B)].

¹²Specifically, a frequency of 11 MHz, a temperature of 304 K, 0% humidity, and various pressures between 26.1–102 kPa were used as inputs, which correspond to Greenspan’s measurements in air over the continuum regime.

from these that the dcE model underpredicts sound attenuation in dry air near room temperature by between approximately 13% and 14%.

Next, let us compare the dcE model's predictions in (4.4) to measurements from PRANGSMA *et al.* [14, Table I] of the quantity, $\alpha p/f^2$, in nitrogen, carbon monoxide, and methane at $T_0 = 293$ K. For this purpose, we use the specific gas constants, $\mathcal{R} = 297, 297,$ and $518 \text{ J} \cdot \text{kg}^{-1} \cdot \text{K}^{-1}$ for nitrogen, carbon dioxide, and methane, respectively, and the values given in Table 2 – the specific heat ratios in the second column are computed with formulas for the isochoric specific heat, c_v , from CALLEN [16, pp. 331–332] evaluated at 293 K and the ideal gas relationship, $\gamma = (c_v + \mathcal{R})/c_v$; the shear viscosities in the third column are taken from [14, Table I]; and the Prandtl numbers in the fourth column are computed with the shear viscosities and thermal conductivities from [14, Table I] and isobaric specific heats, $c_p = 1039, 1036,$ and $2211 \text{ J} \cdot \text{kg}^{-1} \cdot \text{K}^{-1}$ for nitrogen, carbon monoxide, and methane gas, respectively, found by using the ideal gas relationship $c_p = c_v + \mathcal{R}$ and the aforementioned formulas for c_v and values for \mathcal{R} . From the last two columns in Table 2, one again observes the new dcE model shows improvement over the original but in all cases it still underestimates sound attenuation when compared to the experimental measurements. Although we did not use this quantity when computing the dcE model comparison ratios, we present estimates of the bulk-to-shear viscosity ratios in the fifth column of Table 2, which were computed by setting the NSF formula from (4.4) equal to the measured values of $\alpha p/f^2$ in [14, Table I] and solving for ζ/η . These differ a bit from the ones computed directly from the shear and bulk viscosities presented in [14, Table I], indicating that perhaps we have used slightly different values than Prangma *et al.* for c_p and γ .

TABLE 2. Nitrogen, carbon monoxide, and methane data at 293 K from [14].

Gas	γ	η [$\text{kg} \cdot \text{m}^{-1} \cdot \text{s}^{-1}$]	Pr	ζ/η	$\alpha_{\text{dcE(oid)}}/\alpha$	$\alpha_{\text{dcE}}/\alpha$
N ₂	1.40	1.75×10^{-5}	0.713	0.728	0.763	0.824
CO	1.40	1.72×10^{-5}	0.721	0.547	0.821	0.885
CH ₄	1.31	1.09×10^{-5}	0.724	1.29	0.655	0.694

Prangma *et al.* provide a survey of some earlier measurements that were available in the literature at the time to compare with their own. For example in [14, Table II], there appear 12 other experimental measurements done between 1940 and 1970 of $\alpha p/f^2$ in nitrogen near 300 K – one of them being Greenspan's from [13] – and it can be shown that Prangma *et al.*'s value for this quantity is about 3% larger than the average of all the values and about 2% larger than Greenspan's. However, there do not appear to be any large systematic errors in the experiment that would account for the 17.6% difference predicted by the dcE model.

4.4. Liquids

An acoustic spectroscopy technique is used by HOLMES *et al.* [10] to measure sound attenuation in 0.22 μm Millipore water at frequencies ranging between 10 and 100 MHz and at various temperatures between 7°C and 50°C. In Table 3, the first and second columns give the temperatures of the measurements and corresponding ratios of specific heats reported in [10, Table 1]; the Prandtl numbers in the third column are computed using the isobaric specific heat, shear viscosity, and thermal conductivity values given in [10, Table 1]; the bulk-to-shear viscosity ratios in the fourth column are those presented in [10, Table 2]; and the dcE comparison ratios in the last two columns are calculated by dividing their respective formulas in (4.1) by the measured values of α/f^2 from [10, Table 2] and using the water properties presented in [10, Table 1]. Their measurement technique and accompanying error analysis is discussed in [10, Sec. 2], and the errors associated with the bulk viscosities – which, as we recall, are expected to be much higher than errors in the attenuation measurements – are computed at each temperature and reported in [10, Table 2]. There, it is seen that the bulk viscosities are on the order of $10^{-3} \text{ kg} \cdot \text{m}^{-1} \cdot \text{s}^{-1}$ with standard errors on the order of $10^{-5} \text{ kg} \cdot \text{m}^{-1} \cdot \text{s}^{-1}$. In [10, Sec. 3], the authors additionally compare their measurements of bulk viscosity in water to others in the literature and find good overall agreement. From the last two columns of Table 3 one observes the original and newly modified dcE model give similar predictions and they both underestimate sound attenuation in water by more than 51% over the entire temperature range.

TABLE 3. Water data at various temperatures from [10].

T_0 (K)	γ	Pr	ζ/η	$\alpha_{\text{dcE(oid)}}/\alpha$	$\alpha_{\text{dcE}}/\alpha$
280	1.0003	10.5	3.15	0.447	0.446
283	1.0012	9.48	3.08	0.454	0.454
288	1.0035	8.09	2.96	0.466	0.465
298	1.0106	6.11	2.78	0.486	0.483
313	1.0256	4.33	2.82	0.481	0.477
323	1.0386	3.55	2.71	0.492	0.485

In Table 4, data is provided for a few more liquids, each at a temperature of 25°C. The information pertaining to mercury is found in HUNTER *et al.* [17, Tables I and II] – the value of γ is computed by Eq. (3.13) with thermal expansion coefficient, $\alpha_p = 1.817 \times 10^{-4} \text{ K}^{-1}$, and the value for α/f^2 is taken to be the average of the three values at frequencies 90, 150, and 270 MHz. Also, in [17, p. 1570] there appears a discussion of experimental error in which the authors estimate the most probable error in their sound attenuation measurements to be $\pm 1\%$. For ethanol and benzene, the values of α/f^2 are estimates from the

table “Properties of sound in liquids” in [23], and material properties of these liquids are taken from [24–26]. For each liquid, the Prandtl number is computed with the tabulated values of c_p , η , and λ ; the bulk-to-shear viscosity ratio is found by solving the NSF formula in (4.1) for ζ/η and using the tabulated values of α/f^2 ; and the dcE and dcE (old) comparison ratios are calculated by dividing their respective formulas in (4.1) by the tabulated values of α/f^2 . From Table 4, we see that the dcE model gives an accurate prediction of sound attenuation in mercury, and this is a significant improvement over the original dcE model’s estimate, which is about 74% too low. This is because mercury has an unusually low Prandtl number, meaning thermal absorption is the dominant effect in the sound attenuation coefficient, and we recall that in SvÄRD [1] an extra heat flux has been introduced that allows the dcE model to match predictions from Fourier’s law. The results in Table 4 for ethanol are closer to those we see in Table 3 for water – both liquids have relatively high Prandtl numbers and bulk-to-shear viscosity ratios that are greater than 1. The dcE model underestimates sound attenuation in ethanol by about 34%, and the original dcE model gives a somewhat better prediction but is still about 28% too low. The results for benzene in Table 4 show that this liquid has an unusually high bulk viscosity – an estimated 150 times larger than the shear viscosity at 298 K. In this case, we find both the new and original dcE models underpredict sound attenuation by an estimated 99%.

TABLE 4. Mercury, ethanol, and benzene data at 298 K.

Parameter	mercury	ethanol	benzene
ρ_0 [kg/m ³]	1.35×10^4	785	874
c [m/s]	1451	1139	1330
c_p [J · kg ⁻¹ · K ⁻¹]	139	2570	1700
γ	1.15	1.18	1.43
η [kg · m ⁻¹ · s ⁻¹]	1.53×10^{-3}	1.07×10^{-3}	6.04×10^{-4}
λ [W · m ⁻¹ · K ⁻¹]	8.54	0.171	0.143
Pr	0.0249	16.1	7.18
α/f^2 [s ² /m]	5.70×10^{-15}	5.1×10^{-14}	8.7×10^{-13}
ζ/η	0.483	1.5	150
$\alpha_{\text{dcE(ol)}}/\alpha$	0.256	0.72	0.013
$\alpha_{\text{dcE}}/\alpha$	1.00	0.66	0.011

5. Conclusions

We have compared theoretical predictions from the newly revised diffusive compressible Euler model presented in SvÄRD [1] to sound attenuation mea-

measurements in gases and liquids reported in the literature. In doing so, we have shown that the new version of the dcE model now makes accurate predictions of sound propagation in monatomic ideal gases and, when compared to the original dcE model from SVÄRD [2], improved predictions in polyatomic ideal gases. In the latter, however, sound attenuation is still significantly underestimated by the dcE model – for example, in the ideal gases at room temperature studied in Section 4.3, we found that the dcE model underpredicts this quantity by 15%–18% in nitrogen, by 13%–14% in dry air, and by about 9%, 11%, and 31%, in oxygen, carbon monoxide, and methane, respectively. It should be emphasized that all of these predictions lie below the measured data – in other words, the disagreement between the measurements and dcE theory is unlikely to be explained by experimental error, which would be distributed more or less equally above and below the measured quantities, unless there were large systematic errors skewing attenuations in each of these experiments to be too high in polyatomic gases, but not in monatomic gases. This seems implausible. Just as over the course of the last century, acoustic data was used to invalidate Stokes’ hypothesis for general compressible fluids, we may use the same data to argue that the current dcE model appears to lack another transport mechanism. This becomes even more evident when studying liquids. In Section 4.4 we found that, although the revised dcE model gives accurate predictions in mercury, it underestimates sound attenuation in water by more than 51% at all temperatures studied between 7°C and 50°C, and in ethanol and benzene at room temperature by roughly 34% and 99%, respectively.

Appendix A. More on the dispersion relations

First, let us define the dimensionless parameter,

$$(A.1) \quad \delta = \frac{\eta\omega}{\rho_0 c^2},$$

which we recall from Sections 3.1 and 3.2, is assumed to be small when approximating the propagational roots for both the NSF and dcE models. One finds from kinetic gas theory that for the elastic hard-sphere model the mean free path is approximately

$$(A.2) \quad \lambda_{mfp} = \frac{\eta}{\rho_0} \sqrt{\frac{\pi}{2RT_0}},$$

see KENNARD [27, Eq. (126b) on p. 147], and in the continuum regime, this is required to be much smaller than the sound wavelength when there is no dispersion, c/f , and thereby the quantity,

$$(A.3) \quad \lambda_{\text{wave}} = \frac{c}{\omega} = \frac{1}{\beta_0}.$$

Using ideal gas equations (4.3) and (4.6) and definition (A.1), one arrives at the following estimate for the Knudsen number:

$$(A.4) \quad \text{Kn} = \frac{\lambda_{mfp}}{\lambda_{\text{wave}}} = \sqrt{\frac{\pi}{2\gamma}} \frac{1}{r} = \sqrt{\frac{\pi\gamma}{2}} \delta.$$

Therefore, the assumption that δ is a small parameter implies that for ideal gases, our problem lies in the low Knudsen number regime, also known as the continuum regime, i.e., that assumption 5 from Section 2 is satisfied. One generally finds the NSF equations to become inaccurate when Kn is roughly equal to or greater than 0.1, which marks the onset of the transition regime, and in Appendix A.3 this is demonstrated in the case of sound wave propagation.

TABLE 5. Knudsen number regimes.

Flow regime	Kn range
continuum	< 0.1
hydrodynamic	< 0.001
slip	0.001 – 0.1
transition	0.1 – 10
free molecular	> 10

In Table 5, we present some common estimates for the various Knudsen number regimes. These – as well as the definition of the mean free path and Knudsen number, itself – can be subject to some variation throughout the literature. One generally finds the NSF equations to give accurate predictions in the continuum regime, which is defined here as encompassing the hydrodynamic and slip regimes, the latter so-named because accuracy in problems like Poiseuille flow requires the use of tangential velocity slip boundary conditions, see BIRD *et al.* [28, p. 66]. In the continuum regime, fluid behavior is dominated by collisions between molecules, whereas in the free molecular regime, the molecules are at a far enough distance apart that they rarely collide with one another. The transition regime lies between these two extremes. Making accurate predictions outside of the continuum regime generally requires kinetic gas theory models based on the Boltzmann equation.

A.1. Navier–Stokes–Fourier

Using definition (A.1) in (3.14)–(3.16), gives approximate propagational pair,

$$(A.5) \quad k_{pr(\pm)}(\omega) = \pm \frac{\omega}{c} (a_{pr} \delta + i),$$

where we have defined the dimensionless parameter,

$$(A.6) \quad a_{pr} = \frac{2}{3} + \frac{1}{2} \left(\frac{\zeta}{\eta} + \frac{\gamma - 1}{Pr} \right).$$

Under assumption 5, the other approximate root pair of NSF dispersion relation (3.12) is

$$(A.7) \quad k_{th(\pm)}(\omega) = \pm \frac{\omega}{c} \sqrt{\frac{Pr}{2\delta}} ((1 - a_{th}\delta) + i(1 + a_{th}\delta)),$$

where we have defined another dimensionless parameter:

$$(A.8) \quad a_{th} = \frac{\gamma - 1}{2} \left(\frac{4}{3} - \frac{\zeta}{\eta} + \frac{1}{Pr} \right).$$

Note that a_{pr} and a_{th} are both on the order of 1 for ideal gases and many other types of fluids. The roots in (A.7) are referred to as thermal roots, see MORSE and INGARD [29, Ch. 6.4].

Next, let us examine the characteristic attenuation lengths associated with the propagational and thermal roots and compare them. By computing these as the distance it takes for a mode to decay to $1/e$ of its amplitude and using definition (A.3), one finds the approximate propagational and thermal attenuation lengths in the continuum regime to be

$$(A.9) \quad \lambda_{pr} = \frac{1}{|k_{pr(\pm)}|} = \frac{\lambda_{wave}}{a_{pr}\delta}$$

and

$$(A.10) \quad \lambda_{th} = \frac{1}{|k_{th(\pm)}|} = \lambda_{wave} \sqrt{\frac{2\delta}{Pr}} (1 + a_{th}\delta),$$

respectively. Since under assumption 5 it is assumed $\delta \ll 1$, one can see from the above that $\lambda_{pr} \gg \lambda_{wave}$ and the thermal attenuation length is much smaller than the propagational attenuation length (by order $\delta^{3/2}$). To build intuition for the length scales involved in sound experiments conducted in a gas and a liquid, see Tables 5 and 6. In the continuum regime, one finds that away from boundaries, the propagational modes of sound waves dominate. However, depending on the boundary conditions, the thermal modes may play an important role near walls, causing the formation of boundary layers with lengths on the order of λ_{th} , which to leading order is

$$(A.11) \quad \lambda_{th} \sim (c/\omega)\delta^{1/2} = \sqrt{\frac{\eta}{\rho_0\omega}}.$$

A.2. Diffusive compressible Euler

By using definition (A.1) in (3.24) with (3.29) and (3.26), one may express the approximate propagational pair in the dcE model as

$$(A.12) \quad k_{pr(\pm)}(\omega) = \pm \frac{\omega}{c} (b_{pr}\delta + i),$$

where we have defined the dimensionless parameter,

$$(A.13) \quad b_{pr} = 1 + \frac{1}{2}(\gamma - 1) \left(\frac{1}{\text{Pr}} - 1 \right).$$

In the continuum regime, the two other approximate root pairs of dcE dispersion relation (3.23) are found to be

$$(A.14) \quad k_{th(\pm)}(\omega) = \pm \frac{\omega}{c} \sqrt{\frac{\text{Pr}}{2\delta}} ((1 - b_{th}\delta) + i(1 + b_{th}\delta))$$

and

$$(A.15) \quad k_{ex(\pm)}(\omega) = \pm \frac{\omega}{c} b_{ex} \left(\frac{1}{\delta} + ic_{ex} \right),$$

where we have defined three additional dimensionless parameters:

$$(A.16) \quad b_{th} = \frac{(\gamma - 1)(1 - \text{Pr})^3}{2\gamma^{1/2} \text{Pr}^{3/2}},$$

$$(A.17) \quad b_{ex} = \frac{1}{\sqrt{\gamma - (\gamma - 1)\text{Pr}}},$$

and

$$(A.18) \quad c_{ex} = \gamma + \frac{(\gamma - 1)\text{Pr}(\text{Pr} - 3)}{2}.$$

One observes b_{pr} , b_{th} , b_{ex} , and c_{ex} to be on the order of 1 for ideal gases and many other types of fluids. The dcE thermal roots in (A.14) are similar to the NSF thermal roots in (A.7), and we refer to (A.15) as the “extra” root pair¹³.

In the same manner as Appendix A.1, one may use expressions (A.12), (A.14), and (A.15) to compute the characteristic attenuation lengths associated with the propagational, thermal, and extra dcE modes in the continuum regime to find

$$(A.19) \quad \lambda_{pr} = \frac{1}{|k_{pr(\pm)}|} = \frac{\lambda_{\text{wave}}}{b_{pr}\delta},$$

$$(A.20) \quad \lambda_{th} = \frac{1}{|k_{th(\pm)}|} = \lambda_{\text{wave}} \sqrt{\frac{2\delta}{\text{Pr}}} (1 + b_{th}\delta),$$

¹³Note that, depending on the thermodynamic description in which it is cast, the dispersion relation from the NSF model can yield an extra root pair, as well.

and

$$(A.21) \quad \lambda_{ex} = \frac{1}{|k_{ex(\pm)}|} = \frac{\lambda_{wave}\delta}{b_{ex}}.$$

respectively. To leading order, the thermal length is the same in the NSF and dcE models. Note that in the continuum regime, the attenuation length (A.21) corresponding to the extra roots is smaller than the thermal attenuation length. Therefore in this case, by measuring propagational properties at distances from the sound source outside of a potential thermal layer of order (A.11) and (A.20), one is automatically outside of the smaller extra boundary layer that may potentially be present. Further note that the extra attenuation length is independent of the sound frequency and, in ideal gases, proportional to the mean free path.

TABLE 6. Some length scales for argon gas corresponding to experiments in [14].

Parameter	$p = 14.3 \text{ kPa}$	$p = 50.0 \text{ kPa}$	$p = 94.1 \text{ kPa}$
$\lambda_{mfp} [\mu\text{m}]$	0.503	0.144	0.0787
Kn	0.107	0.0307	0.0163
$\lambda_{pr} [\mu\text{m}]$	60.6 (NSF) 60.6 (dcE)	212 (NSF) 212 (dcE)	398 (NSF) 398 (dcE)
$\lambda_{th} [\mu\text{m}]$	2.22 (NSF) 2.09 (dcE)	1.14 (NSF) 1.12 (dcE)	0.824 (NSF) 0.816 (dcE)
$\lambda_{ex} [\mu\text{m}]$	0.344 (dcE)	0.0983 (dcE)	0.0524 (dcE)

TABLE 7. Some length scales for water at room temperature corresponding to experiments in [12].

Parameter	$f = 10 \text{ MHz}$	$f = 50 \text{ MHz}$	$f = 100 \text{ MHz}$
$\lambda_{wave} [\mu\text{m}]$	23.8	4.67	2.38
δ	2.50×10^{-5}	1.25×10^{-4}	2.50×10^{-4}
$\lambda_{pr} [\text{mm}]$	463 (NSF) 958 (dcE)	18.5 (NSF) 38.3 (dcE)	4.63 (NSF) 9.58 (dcE)
$\lambda_{th} [\mu\text{m}]$	0.0681 (NSF) 0.0681 (dcE)	0.0300 (NSF) 0.0300 (dcE)	0.0215 (NSF) 0.0215 (dcE)
$\lambda_{ex} [\text{nm}]$	0.579 (dcE)	0.579 (dcE)	0.579 (dcE)

Tables 6 and 7 are provided to give a sense of the above length scales involved in sound wave experiments conducted in gases and liquids. In Table 6, we use parameters corresponding to the measurements in argon from GREENSPAN [12]. At $T_0 = 303 \text{ K}$ with $\gamma = 5/3$ and $\mathcal{R} = 208 \text{ J} \cdot \text{kg}^{-1} \cdot \text{K}^{-1}$ for argon, we use the ideal gas equation (4.3) to calculate a sound speed of $c = 324 \text{ m/s}$, which together with the ultrasound frequency $f = 11 \text{ MHz}$ yields a characteristic wavelength

(divided by 2π) of $\lambda_{\text{wave}} = 4.69 \mu\text{m}$. Table 6 contains length scales corresponding to three pressures spanning Greenspan’s argon data in the continuum regime. We additionally use the values, $\text{Pr} = 2/3$, $\zeta = 0$, and $\eta = 2.29 \times 10^{-5} \text{ kg} \cdot \text{m}^{-1} \cdot \text{s}^{-1}$ from Sutherland’s formula evaluated at 303 K with constants in [12, Table I], and the ideal gas relationship, $\rho_0 = p/(\mathcal{R}T_0)$. In Table 7, the parameters for water at 25°C from HOLMES *et al.* [10, Table 1] are used to compute the length scales corresponding to three frequencies spanning the range employed in their measurements.

A.3. Rarefied gas regime

As explained in Section 4.1 and the beginning of this appendix, both the NSF and dcE models are systems of balance laws formulated in the continuum regime and, therefore should not be expected to perform well for problems involving Knudsen numbers roughly above 0.1. It is interesting to note, however, that exact roots may be computed from both the NSF and dcE dispersion relations (3.12) and (3.23), enabling us to observe the models’ predictions outside of the continuum regime. The resulting equations are rather lengthy and so we will not present them in closed form here. However, in Fig. 7 we plot the NSF and dcE predictions for the quantities, α/β_0 and β/β_0 , corresponding to the exact propagational roots, $k_{pr(\pm)}$, together with the complete set of argon measurements

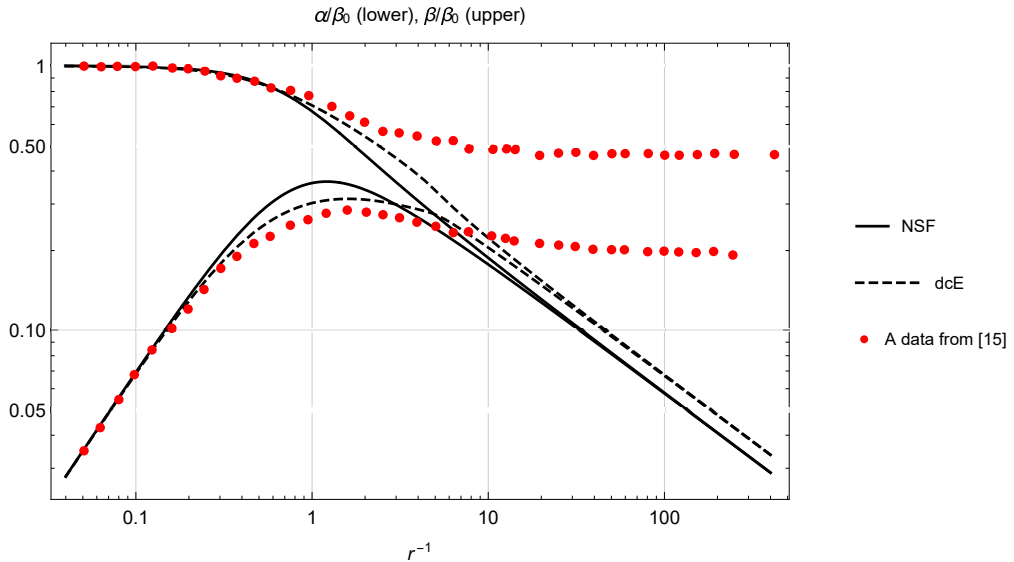


FIG. 7. Dimensionless sound attenuation coefficient and dimensionless inverse sound speed vs. dimensionless rarefaction parameter: data and theoretical predictions in argon gas at 296 K.

from SCHOTTER [15, Fig. 8]. Note that by using (A.4) with $\gamma = 5/3$ for noble gases, we find that in this example, the Knudsen number is slightly less than r^{-1} and computed as approximately $\text{Kn} = 0.971 \times r^{-1}$. In Fig. 7, we can see that the transition regime begins somewhere between the values $r^{-1} = 0.1$ and 0.2 , where the measurements of α/β_0 and β/β_0 start to deviate from linear and decrease below 1, respectively; and the free molecule regime begins at about $r^{-1} = 10$, where the measurements of α/β_0 and β/β_0 both begin to level off. One notices, as expected, that the theoretical predictions both become inaccurate outside of the continuum regime – especially for the parameter, β/β_0 – but that in this example, the dcE model gives better predictions than the NSF equations in the transition regime and may be used with reasonable accuracy out to a value of about $r^{-1} = 0.3$. On the other hand, recall that the dcE model gives accurate continuum regime predictions for sound attenuation only in noble gases, and so the improvement seen here for argon is not of a general nature.

Acknowledgements

My father, Dr. Marvin E. Morris, digitized the data presented in Figs. 2–7, obtained most of the references in the bibliography, and taught me valuable information about equipment used in the various acoustic experiments discussed here. Moreover, upon studying the University of Michigan reports of Uhlenbeck and Wang Chang, he challenged me many years ago to compare my own alternate fluid model's predictions with acoustic data, for which I am very grateful.

References

1. M. SVÄRD, *Refining the diffusive compressible Euler model*, *Physica A*, **635**, 129474, 2024.
2. M. SVÄRD, *A new Eulerian model for viscous and heat conducting compressible flows*, *Physica A*, **506**, 350–375, 2018.
3. V. DOLEJŠÍ, M. SVÄRD, *Numerical study of two models for viscous compressible fluid flows*, *Journal of Computational Physics*, **427**, 110068, 2021.
4. M.L. MORRIS, *Analysis of an alternative Navier-Stokes system: attenuation of sound waves*, ResearchGate preprint, doi: 10.13140/RG.2.2.29383.01442, 2021.
5. M.L. MORRIS, *Analysis of an alternative Navier-Stokes system: Rayleigh-Brillouin light scattering*, ResearchGate preprint, doi: 10.13140/RG.2.2.32239.92321, 2022.
6. M.L. MORRIS, *Heat conduction in a new Eulerian flow model*, *Archives of Mechanics*, **76**, 1-2, 191–202, 2024.
7. M. SVÄRD, K. MUNTHE, *A study of the diffusive properties of a modified compressible Navier-Stokes model*, *Meccanica*, **58**, 1083–1097, 2023.
8. A.B. BHATIA, *Ultrasonic Absorption: An Introduction to the Theory of Sound Absorption and Dispersion in Gases, Liquids and Solids*, Dover, New York, 1967.

9. M.R. MOLDOVER, J.B. MEHL, M. GREENSPAN, *Gas-filled spherical resonators: theory and experiment*, Journal of the Acoustical Society of America, **79**, 2, 253–272, 1986.
10. M.J. HOLMES, N.G. PARKER, M.J.V. POVEY, *Temperature dependence of bulk viscosity in water using acoustic spectroscopy*, Journal of Physics: Conference Series, **269**, 012011, 2011.
11. Z. GU, W. UBACHS, *Temperature-dependent bulk viscosity of nitrogen gas determined from spontaneous Rayleigh-Brillouin scattering*, Optics Letters, **38**, 7, 1110–1112, 2013.
12. M. GREENSPAN, *Propagation of sound in five monatomic gases*, Journal of the Acoustical Society of America, **28**, 4, 644–648, 1956.
13. M. GREENSPAN, *Rotational relaxation in nitrogen, oxygen, and air*, Journal of the Acoustical Society of America, **31**, 2, 155–160, 1959.
14. G.J. PRANGSMA, A.H. ALBERGA, J.J.M. BEENAKKER, *Ultrasonic determination of the volume viscosity of N₂, CO, CH₄, and CD₄ between 77 and 300 K*, Physica, **64**, 278–288, 1973.
15. R. SCHOTTER, *Rarefied gas acoustics in the noble gases*, Physics of Fluids, **17**, 6, 1163–1168, 1974.
16. H.B. CALLEN, *Thermodynamics*, John Wiley & Sons, New York, London, 1962.
17. J.L. HUNTER, T.J. WELCH, C.J. MONTROSE, *Excess absorption in mercury*, Journal of the Acoustical Society of America, **35**, 10, 1568–1570, 1963.
18. https://www.engineeringtoolbox.com/nitrogen-d_1421.html, March 28, 2024.
19. https://www.engineeringtoolbox.com/oxygen-d_1422.html, March 28, 2024.
20. https://www.engineeringtoolbox.com/dry-air-properties-d_973.html, March 28, 2024.
21. <http://www.cgsnetwork.com/atmosndabsorbcalc.html>, March 25, 2024.
22. <https://resource.npl.co.uk/acoustics/techguides/absorption>, March 25, 2024.
23. http://www.kayelaby.npl.co.uk/general_physics/2_4/2_4_1.html, June 15, 2012.
24. https://www.engineeringtoolbox.com/ethanol-ethyl-alcohol-properties-C2H6O-d_2027.html, March 28, 2024.
25. https://www.engineeringtoolbox.com/thermal-conductivity-liquids-d_1260.html, March 28, 2024.
26. https://www.engineeringtoolbox.com/benzene-benzol-properties-d_2053.html, March 28, 2024.
27. E.H. KENNARD, *Kinetic Theory of Gases With an Introduction to Statistical Mechanics*, McGraw-Hill, New York, London, 1938.
28. R.B. BIRD, W.E. STEWART, E.N. LIGHTFOOT, *Transport Phenomena*, 2nd ed., John Wiley, New York, 2002.
29. P.M. MORSE, K.U. INGARD, *Theoretical Acoustics*, Princeton University Press, Princeton, New Jersey, 1986.

Received April 9, 2024; revised version July 9, 2024.

Published online August 9, 2024.
